JOURNAL OF GUIDANCE, CONTROL, AND DYNAMICS
Vol. 15, No. 2, March-April 1992

Probabilities of Escape, Re-Entry, and Orbit Decay Due to Misdirected Injection Maneuvers

James M. Longuski*
Purdue University, West Lafayette, Indiana 47907

Whenever a space vehicle is injected from low Earth orbit to high orbit or to escape, there is a small probability of misdirection. Once misdirection is assumed, then up to three major families of trajectories may result: escape, re-entry, or orbit decay. Analytic models of these trajectories provide contours on the injection sphere. Analytic integration of the areas between the contours gives the relative probability of each family occurring. The approximate analytic models are much faster in providing solutions than the numerical methods currently in use and have comparable accuracy. The new method provides a useful tool in the safety analysis of both single and multistage injection maneuvers. Recent applications have included analysis of the Galileo and the Ulysses injections into interplanetary trajectories.

Introduction

RECENTLY there has been much concern about safety issues related to the launchings of nuclear powered spacecraft. Traditionally, a considerable amount of analysis is performed for each individual launch. An important aspect of the safety analysis involves the injection maneuver from low Earth orbit, which puts the vehicle into a high-energy elliptic orbit or an interplanetary trajectory. The injection maneuver is typically very large and may involve a single stage, as in the cases of the early plans of injecting the Galileo and Ulysses spacecraft with the wide-body Centaur upper stage,[1-3] or it may involve multiple stages with time delays between staging, as in the case of the actual Galileo launch in 1989 with the inertial upper stage (IUS).[4]

Clearly, misdirection of the injection maneuver could result in re-entry of the vehicle. However, the probability of a very large error in the injection attitude of the vehicle is considered to be extremely small (less than 1 in 10^6, for example). For the purpose of this analysis, it is assumed that this highly unlikely event has occurred and that the pointing attitude during the misdirected maneuver is held inertially fixed (by the attitude control system) but is a random variable, evenly distributed over the sphere of possible directions. Other assumptions may be equally valid, such as allowing that the maneuver may not be controlled in attitude and may not be completed. The analysis that follows could be used to support these and other possible assumptions, but for the sake of consistency with previous analyses,[1-4] the assumption of a complete, inertially fixed but misdirected burn will be adhered to.

Three major families of trajectories may result from a misdirected injection maneuver: escape, re-entry or orbit decay. Re-entry families are further divided into powered entries, in which the vehicle is still thrusting, and delayed entries, in which burnout has already occurred. Orbit decay families, of course, also result in eventual re-entry. The purpose of studying these various families is to support the breakup analysis of the vehicle,[1,2] which is very different for each type of entry. Powered entries are potentially the most catastrophic because of the possibility that the remaining propellant may explode. Orbit decay trajectories result in the lowest entry speeds and are considered less dangerous.

Presented as Paper 88-4245 at the AIAA/AAS Astrodynamics Conference, Minneapolis, MN, Aug. 15-17, 1988; received Feb. 9, 1989; revision received Jan. 3, 1991; accepted for publication Feb. 9, 1991.

*Assistant Professor, School of Aeronautics and Astronautics. Senior Member AIAA.

So far, only numerical methods have been used to identify the trajectory families. The method is tedious, involving simulation of hundreds of trajectories. In this paper, analytic methods are presented in which the explicit contours dividing the various trajectory families are found. Analytic integration between the contours provide the relative probabilities of escape, orbit decay, powered entries, and delayed entries. The organization is as follows. First, an impulsive injection analysis is developed that provides geometric contours on the injection sphere. Second, a finite-burn analysis is presented, which is based on the analytic solution of Hill's equations of relative motion. Third, the geometric and analytic solutions are used in a numerical application (Ulysses injection) and compared with the standard numerical approach. Finally, conclusions are drawn about the accuracy and speed of the new method.

Impulsive Injection Analysis

Velocity Sphere

Figure 1 illustrates the velocity sphere of all possible injection orientations from circular orbit. The radius of the sphere is equal to a constant V_I. For a specific injection the orientation of V_I is defined by a cone angle A and a clock angle B.

The clock angle B is measured from the local horizontal plane by way of a right-hand rule rotation about the circular

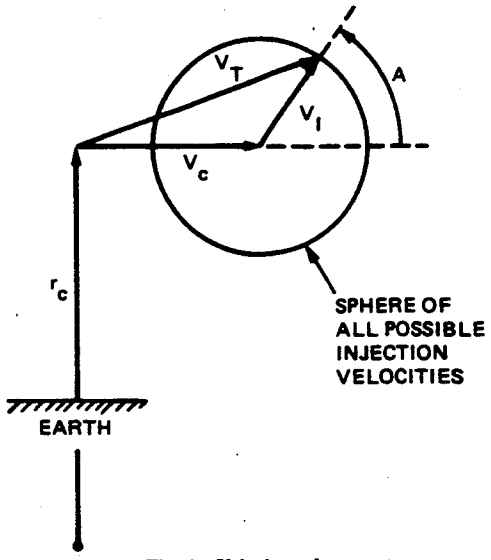

Fig. 1 Velocity sphere.

velocity vector V_c, and is equal to 90 deg in Fig. 1. The vectorial addition of V_c and V_I give the total velocity vector V_T.

Escape Cone

We will now consider the escape trajectories resulting from spherically distributed injection errors.

Since

$$V_{esc} = 2^{1/2} V_c \tag{1}$$

and from the law of cosines

$$V_{esc}^2 = V_c^2 + V_I^2 + 2V_c V_I \cos A_{esc} \tag{2}$$

we obtain from Eqs. (1) and (2)

$$A_{esc} = \cos^{-1}\left[(V_c^2 - V_I^2)/(2V_c V_I)\right] \tag{3}$$

where A_{esc} is the cone angle of escape, which ranges from 0 to 180 deg. The fractional area S_{esc}, encompassed by the escape cone, is given by

$$S_{esc} = (1 - \cos A_{esc})/2 \tag{4}$$

Clearly, all trajectories with cone angles less than or equal to A_{esc} have the necessary energy for escape. However, not all of these cases result in actual escape because those having negative flight path angles may re-enter before or during the pass through periapsis. For low Earth orbit, nearly half of the trajectories with escape energy will re-enter.

Thus, a more complex problem arises, namely the identification of the contour separating the re-entry and escape trajectories (among the escape energy cases) and the integration of the area bounded by the upper half escape cone and the contour in question.

For simplicity it is assumed that any trajectory with a periapsis equal to or below the atmosphere boundary (assumed here to be at an altitude of 400,000 ft) will result in re-entry. Thus, we are interested in the families of trajectories having constant periapsis, which will be referred to as isoperiapsis contours.

Isoperiapsis Contours

The isoperiapsis contour is used to divide the escape cone into two regions: trajectories that escape and trajectories that re-enter due to a periapsis lower than or at the atmosphere boundary.

Consider the family of trajectories with $r_p = \text{const}$. The energy and angular momentum equations are

$$H = r_c V_T \cos\gamma_T = r_p V_p \tag{5}$$

$$E = (V_T^2/2) - (\mu/r_c) = (V_p^2/2) - (\mu/r_p) \tag{6}$$

where r_p and V_p are the periapsis radius and periapsis velocity, respectively. Since we are interested in isoperiapsis contours, r_p is assumed to be constant in Eqs. (5) and (6), but H and E are not assumed to be constant for the various families of trajectories under consideration, since V_T is a varying function of the cone angle A:

$$V_T = (V_c^2 + 2V_c V_I \cos A + V_I^2)^{1/2} \tag{7}$$

The flight path angle γ_T is a function of both cone angle A and the clock angle B:

$$\gamma_T = \sin^{-1}\left[(V_I/V_T)\sin A \sin B\right] \tag{8}$$

(In Fig. 1, γ_T is the angle between V_c and V_T, when $B = 90$ deg.)

Thus for isoperiapsis contours, the only two constants in Eqs. (5) and (6) are r_p and μ/r_c as the cone and clock angles A and B are permitted to vary for different injections.

Eliminating V_p from Eqs. (5) and (6), we obtain

$$(V_T^2/2)\left[1 - (r_c/r_p)^2 \cos^2\gamma_T\right] = (\mu/r_c) - (\mu/r_p) \tag{9}$$

We will now write $V_T = V_T(A)$ and $\gamma_T = \gamma_T(A, B)$. The result from Eqs. (7), (8), and (9) is

$$a \cos A + b = \sin^2 A \sin^2 B \tag{10}$$

where

$$a = 2(V_c/V_I)\left[1 - (r_p/r_c)^2\right]$$

$$b = \left[1 + (V_c/V_I)^2\right]\left[1 - (r_p/r_c)^2\right] - \left(2\mu/V_I^2\right)(r_p/r_c)^2\left(r_p^{-1} - r_c^{-1}\right)$$

Let us put Eq. (10), which is the equation of the isoperiapsis contour, in xyz coordinates of Fig. 1 where the x axis points along the circular position vector r_c, the y axis points along the circular velocity vector V_c, and the z axis points into the page.

Then the transformation equations for the unit sphere become

$$x = \sin A \sin B \tag{11}$$

$$y = \cos A \tag{12}$$

$$z = \sin A \cos B \tag{13}$$

so that Eq. (10) can be put in the form

$$ay + b = x^2 \tag{14}$$

where a and b are constants.

Thus the equation of the isoperiapsis contours is the equation of a parabola in the xy plane. Figure 2 illustrates the geometric interpretation of the isoperiapsis contours: the intersection of the sphere of injection velocities with a parabolic cylinder that extends along the plus and minus z directions.

Areas (Probabilities) on the Velocity Sphere

If we assume that the injection velocity is evenly distributed over the velocity sphere, then the areas between contours on the sphere correspond to probabilities. Figures 3 and 4 illustrate the various families of trajectories resulting from a misdirected injection.

The shaded area under the isoperiapsis contour and above the escape contour corresponds to hyperbolic entries, which are trajectories with escape velocity or greater but with periapsis lower than or equal to the atmosphere and with initial flight-path angles that are negative.

The calculation of the area of actual escape trajectories is trivial: subtract the area of the hyperbolic entries from the area

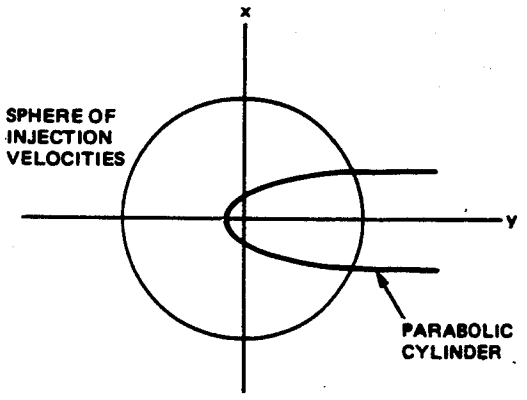

Fig. 2 Parabolic cylinder for isoperiapsis contours.

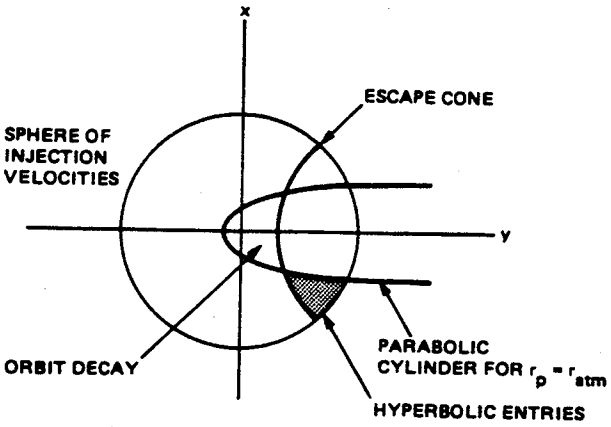

Fig. 3 Trajectory families (side view).

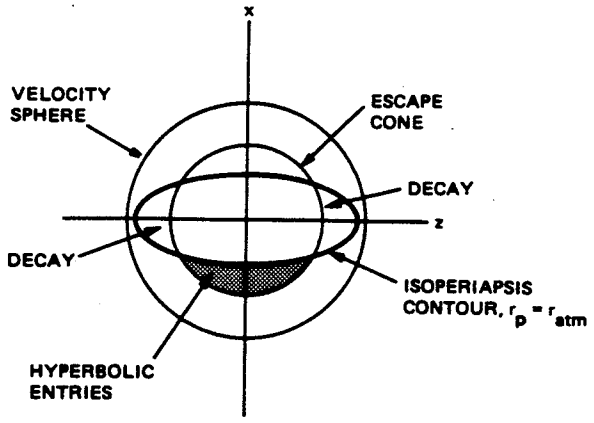

Fig. 4 Trajectory families (front view).

of the escape cone. The area of the cases of orbit decay involves another integration under the isoperiapsis contour and bounded by the escape cone. These are the cases in which the orbit is elliptic and the periapsis is above or at the atmosphere. All remaining cases are elliptic with periapsis lower than the atmosphere, so they involve prompt or delayed entries corresponding to negative and positive initial flight-path angles, respectively. Some of the prompt cases are powered entries, which will be discussed in the next section.

The method of finding the areas is straightforward; for example, the fractional area for the hyperbolic entries is[3]

$$S_{\text{hyp}} = \frac{1}{2\pi}\int_{A(-90\text{ deg})}^{A_{\text{esc}}}\int_{B(A_{\text{esc}})}^{B(A)} \sin A\,dB\,dA \tag{15}$$

where $B(A)$ is found from Eq. (10):

$$B(A) = \sin^{-1}\left[(a\cos A + b)^{1/2}/\sin A\right] \tag{16}$$

and $A(-90\text{ deg})$ is the value of A for $B = -90$ deg on the isoperiapsis contour [the inverse function of $B(A)$]:

$$A(-90\text{ deg}) = \cos^{-1}\left(\left\{-a + \left[a^2 - 4(b-1)\right]^{1/2}\right\}/2\right) \tag{17}$$

However, the evaluation of these integrals may involve infinite series of the elliptic integrals.[3]

Methods to approximate the integrals for the area of hyperbolic entries and the area of orbit decay will be discussed in the section on numerical applications.

Finite-Burn Analysis

The analysis of powered entries cannot be achieved with impulsive maneuvers because an essential issue of the powered-entry problem is the time of entry, which provides an estimate of remaining propellant on board the injection vehicle.

To analyze powered entries, we will use Hill's equations of relative motion[5] (or Clohessy-Wiltshire equations). An important application of these equations is the rendezvous problem in which a spacecraft maneuvers toward a target vehicle in circular orbit within a specified period of time. In the powered-entry analysis, we use Hill's equations to "rendezvous" with the atmosphere at a given time. To perform the analysis, Hill's equations of motion are analytically integrated for a forcing function consisting of a series of step functions, which represent multiple staging. The burn times and delay times between stages are arbitrary as are the number of possible stages and the thrust of each stage. Average accelerations for each stage are found by dividing the total velocity change for each stage by the burn duration.

The results are rather surprising. It is shown that the families of powered entries for a specified entry time fall on circles on the acceleration sphere.[3,4] Even though linear equations of motion are used, these results are in close agreement with simulations.

Hill's Equations of Relative Motion (Clohessy-Wiltshire Equations)

If we assume an inertially fixed, misdirected injection maneuver, then Hill's equations are[3]

$$\ddot{x} - 2n\dot{y} - 3n^2x = a_X\cos nt + a_Y\sin nt \tag{18}$$

$$\ddot{y} + 2n\dot{x} = a_Y\cos nt - a_X\sin nt \tag{19}$$

$$\ddot{z} + n^2z = a_Z \tag{20}$$

where $n = V_c/r_c$, the x axis points along the circular position vector r_c, the y coordinate is aligned with the circular velocity vector V_c, and the z axis points into the page of Fig. 1.

To model the multistaging, we assume that the accelerations come in step functions as follows:

$$a_X = \sum_{k=1}^{m} a_{X_k}\left[h(t-T_{ki}) - h(t-T_{kf})\right] \tag{21}$$

$$a_Y = \sum_{k=1}^{m} a_{Y_k}\left[h(t-T_{ki}) - h(t-T_{kf})\right] \tag{22}$$

$$a_Z = \sum_{k=1}^{m} a_{Z_k}\left[h(t-T_{ki}) - h(t-T_{kf})\right] \tag{23}$$

where $h(t) = 0$, $t < 0$; $h(t) = 1$, $t \geq 0$ (step function), m = total number of stages, a_{X_k} = average acceleration of the kth stage along the X inertial coordinate, T_{ki} = time of ignition of the kth stage, and T_{kf} = burnout (or final) time of the kth stage.

The average acceleration is found by the rocket equation[6] for ΔV

$$a_k = \Delta V_k/(T_{kf} - T_{ki}) = I_{\text{sp}_k} g\,\ln(m_{ki}/m_{kf})/(T_{kf} - T_{ki}) \tag{24}$$

where I_{sp_k} = specific impulse of the kth stage, m_{ki} = initial mass of the kth stage, and m_{kf} = final mass of the kth stage.

Analytic Integration of Hill's Equations

Combining Eqs. (20) and (23), the differential equation for z is

$$\ddot{z} + n^2z = \sum_{k=1}^{m} a_{Z_k}\left[h(t-T_{ki}) - h(t-T_{kf})\right] \tag{25}$$

We will assume zero initial conditions:

$$z(0) = \dot{z}(0) = 0 \tag{26}$$

Care must be exercised when integrating differential equations with step functions, which are in the class of generalized functions. Kaplan[7] discusses the theory of generalized functions in his book on operational methods. The theory is ideally suited to the solution of Eqs. (18–23), as follows.

For Eq. (25), Kaplan defines the operator $T_0[f]$ for zero initial values:

$$T_0[f] = \frac{1}{n}\int_0^t \sin n(t-u) f(u)\,du \tag{27}$$

Putting

$$f(u) = h(u-a) \tag{28}$$

into Eq. (27), we obtain

$$T_0\big[h(t-a)\big] = (1/n^2)\Big\{1-\cos\big[n(t-a)\big]\Big\}h(t-a) \tag{29}$$

Since Eq. (25) is linear, the solution from Eq. (29) is

$$z = \sum_{k=1}^{m} a_{Z_k}\frac{1}{n^2}\left(\Big\{1-\cos\big[n(t-T_{ki})\big]\Big\}h(t-T_{ki}) - \Big\{1-\cos\big[n(t-T_{kf})\big]\Big\}h(t-T_{kf})\right) \tag{30}$$

To integrate Eq. (18), we must first perform a single integration of Eq. (19) to obtain $\dot{y}$ and then substitute the expression for $\dot{y}$ into Eq. (18) to decouple Eqs. (18) and (19). We obtain for $\dot{y}$

$$\dot{y} = -2nx + \frac{1}{n}\sum_{k=1}^{m} a_{Y_k}\big[(\sin nt - \sin nT_{ki})h(t-T_{ki}) - (\sin nt - \sin nT_{kf})h(t-T_{kf})\big] + \frac{1}{n}\sum_{k=1}^{m} a_{X_k}\big[(\cos nt - \cos nT_{ki})h(t-T_{ki}) - (\cos nt - \cos nT_{kf})h(t-T_{kf})\big] \tag{31}$$

Substituting Eq. (31) into Eq. (18) gives the forced harmonic oscillator form

$$\ddot{x} + n^2 x = \sum_{k=1}^{m}\Big\{a_{X_k}\big[3c(h_i-h_f) - 2(c_i h_i - c_f h_f)\big] - a_{Y_k}\big[3s(h_i-h_f) - 2(s_i h_i - s_f h_f)\big]\Big\} \tag{32}$$

where we have introduced the notation

$$h_i = h(t-T_{ki}), \qquad h_f = h(t-T_{kf})$$
$$c = \cos nt, \qquad s = \sin nt$$
$$c_i = \cos nT_{ki}, \qquad c_f = \cos nT_{kf}$$
$$s_i = \sin nT_{ki}, \qquad s_f = \sin nT_{kf}$$

the solution of

$$\ddot{x} + n^2 x = f(t) \tag{33}$$

$$x(0) = \dot{x}(0) = 0$$

$$f(t) = h(t-a),$$

$$h(t-a)\cos nt, \text{ or}$$

$$h(t-a)\sin nt$$

Then the operator T_0, from Eq. (27) gives

$$T_0\big[h(t-a)\big] = (1/n^2)\big[1-\cos n(t-a)\big]h(t-a) \tag{34}$$

$$T_0\big[h(t-a)\cos nt\big] = (1/2n^2)\big[n(t-a)\sin nt - \sin na\,\sin n(t-a)\big]h(t-a) \tag{35}$$

$$T_0\big[h(t-a)\sin nt\big] = (1/2n^2)\big[\sin nt - n(t-a)\cos nt - \sin na\,\cos n(t-a)\big]h(t-a) \tag{36}$$

Thus, the multistage solution for $x(t)$ is

$$x(t) = \frac{1}{n^2}\sum_{k=1}^{m}\left\{a_{X_k}\left[\frac{3}{2}(N_i s - s_i S_i)h_i - \frac{3}{2}(N_f s - s_f S_f)h_f - 2c_i(1-C_i)h_i + 2c_f(1-C_f)h_f\right] + a_{Y_k}\left[\frac{3}{2}(s - N_i c - s_i C_i)h_i - \frac{3}{2}(s - N_f c - s_f C_f)h_f - 2s_i(1-C_i)h_i + 2s_f(1-C_f)h_f\right]\right\} \tag{37}$$

where we have introduced additional notation

$$C_i = \cos n(t-T_{ki}), \qquad C_f = \cos n(t-T_{kf})$$
$$S_i = \sin n(t-T_{ki}), \qquad S_f = \sin n(t-T_{kf})$$
$$N_i = n(t-T_{ki}), \qquad N_f = n(t-T_{kf})$$

By substituting Eq. (37) into Eq. (31) and integrating, we obtain $y(t)$:

$$y(t) = \frac{1}{n^2}\sum_{k=1}^{m}\Big\{a_{X_k}\big[3(N_i c - s + s_i)h_i - 3(N_f c - s + s_f)h_f + 3s_i(1-C_i)h_i - 3s_f(1-C_f)h_f + 3(c_i N_i h_i - c_f N_f h_f) - 4(c_i S_i h_i - c_f S_f h_f) + (s-s_i)h_i - (s-s_f)h_f\big] + a_{Y_k}\big[2(c-c_i)h_i - 2(c-c_f)h_f + 3(N_i s + c - c_i)h_i - 3(N_f s + c - c_f)h_f - s_i S_i h_i + s_f S_f h_f + 3(s_i N_i h_i - s_f N_f h_f)\big]\Big\} \tag{38}$$

Isochrone Contours

By setting the relative altitude equation, Eq. (37), equal to the relative altitude of the atmosphere at a given time, we obtain the equation of isochrone (fixed-time) contours:

$$x(t_{\text{atm}}) = x_{\text{atm}} \tag{39}$$

Note that since the relative altitude of the atmosphere is below the circular orbit, Eq. (39) gives a negative value. Equation (37) can be put in the form

$$x(t_{\text{atm}}) = \sum_{k=1}^{m} a_{X_k} f_{X_k}(t_{\text{atm}}) + a_{Y_k} f_{Y_k}(t_{\text{atm}}) \tag{40}$$

Suppose that the initial stage direction is given $(a_{X_1}, a_{Y_1}, a_{Z_1})$ and that the directions of the succeeding stages are determined by (some relationships to) the first-stage direction. Then Eq. (40) can be rewritten as

$$x(t_{\text{atm}}) = a_{X_1}\sum_{k=1}^{m}\bar{a}_{X_k} f_{X_k}(t_{\text{atm}}) + a_{Y_1}\sum_{k=1}^{m}\bar{a}_{Y_k} f_{Y_k}(t_{\text{atm}}) \tag{41}$$

where we have introduced the scaled accelerations

$$\tilde{a}_{X_k} = a_{X_k}/a_{X_1} \tag{42}$$

$$\tilde{a}_{Y_k} = a_{Y_k}/a_{Y_1} \tag{43}$$

and where $\tilde{a}_{X_1} = \tilde{a}_{Y_1} = 1$. We assume that the scaled variables in Eqs. (42) and (43) are known parameters.

If we define new functions

$$g_X(t_{\text{atm}}) = \sum_{k=1}^{m} \tilde{a}_{X_k} f_{X_k}(t_{\text{atm}}) \tag{44}$$

$$g_Y(t_{\text{atm}}) = \sum_{k=1}^{m} \tilde{a}_{Y_k} f_{Y_k}(t_{\text{atm}}) \tag{45}$$

then

$$x(t_{\text{atm}}) = a_{X_1} g_X(t_{\text{atm}}) + a_{Y_1} g_Y(t_{\text{atm}}) \tag{46}$$

Since g_X and g_Y are known functions of t_{atm}, Eq. (46) is the equation of a line as before in the single-state case.[3,4] In our application to the Galileo and Ulysses problems, we assume the directions of all the stages will be the same.

Table 1 Ulysses injection at 110 n.mi.

Event	Time, s	Weight, lb	I_{sp}, s
Burn 1	0–152	38,676–17,033	293.3
Coast 1	152–212		
Burn 2	212–315.4	14,593–8,519	301.2
Coast 2	315.4–375.4		
Burn 3	375.4–460.4	5,914–1,415	292.1

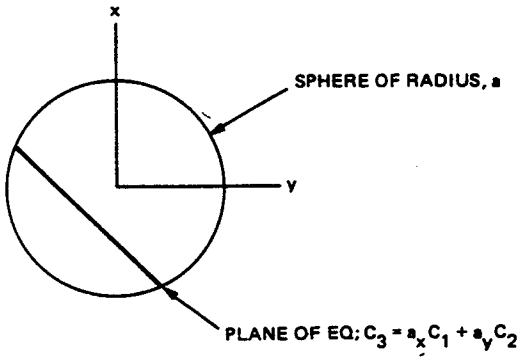

Fig. 5 Acceleration sphere.

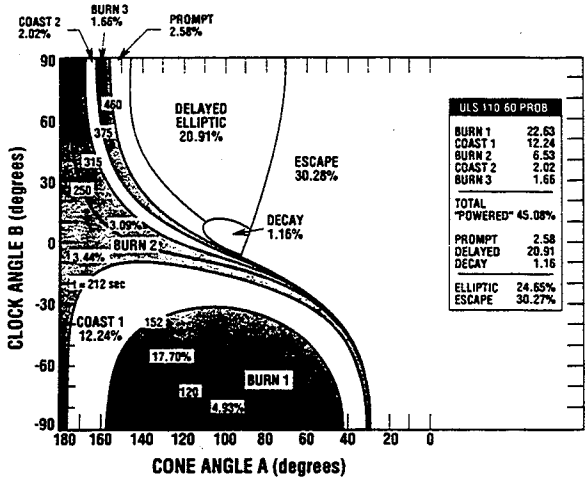

Fig. 6 Fixed misdirected burn map for Ulysses (numerical solution) for 110 n.mi. orbit.

Equation (46) not only applies to these problems but also t cases in which the succeeding stages are misaligned in differer fixed directions. Thus the linear equation [Eq. (46)] is an im portant general result.

Figure 5 illustrates this result. The isochrone contours ar represented as planar cuts through the acceleration sphere o circles on the sphere.

Velocity Components

The absolute velocity components in xyz coordinates are given by

$$V_x = \dot{x} \tag{47}$$

$$V_y = \dot{y} + V_c + nx \tag{48}$$

$$V_z = \dot{z} \tag{49}$$

A convenient expression for $\dot{y}$ is found in Eq. (31). The expressions for $\dot{x}$ and $\dot{z}$ are found by differentiating Eqs. (37) and (30) (note that the delta functions that arise from differentiation are of no consequence to physical systems[7] and so will be ignored):

$$\dot{x}(t) = \frac{1}{n}\sum_{k=1}^{m}\left\{a_{X_k}\left[\frac{3}{2}(s + N_i c - s_i C_i)h_i - \frac{3}{2}(s + N_f c - s_f C_f)h_f - 2(c_i S_i h_i - c_f S_f h_f)\right] + a_{Y_k}\left[\frac{3}{2}(N_i s + s_i S_i)h_i - \frac{3}{2}(N_f s + s_f S_f)h_f - 2(s_i S_i h_i - s_f S_f h_f)\right]\right\} \tag{50}$$

$$\dot{z}(t) = \frac{1}{n}\sum_{k=1}^{m} a_{Z_k}\left[S_i h_i - S_f h_f\right] \tag{51}$$

Numerical Application

We will now compare the analytic models to the standard numerical approach for the specific case of the Ulysses spacecraft injection from an orbit of 110 n.mi. As shown in Table 1, the injection involves three stages with long coast times (60 s) in between.

Figure 6 presents the numerical results that are found by making approximately 250 trajectory simulations of misdirected injection maneuvers, where each trajectory simulation corresponds to a particular pair of values for clock and cone angles (B,A). After categorizing each trajectory type (escape, powered entry, orbit decay, etc.), the burn map of clock angle vs cone angle is drawn by connecting line segments that separate the families of trajectories. A numerical integration of areas between the line segment contours is then performed.[1,2] The entire process requires about two man-weeks of effort.

Figure 7 presents the results of the analytic methods developed previously. The amount of effort required is of the order of a few minutes (the time required to run a short computer program and plot the results). The enormous reduction in effort is due primarily to the fact that all the analytic solutions are closed form so that no numerical integration or trajectory propagation of any kind is required.

Certain approximations are used in producing the analytic burn map. For the escape trajectories, the area is approximated by

$$S_{\text{esc}} \approx f(1 - \cos A_{\text{esc}})/2 \tag{52}$$

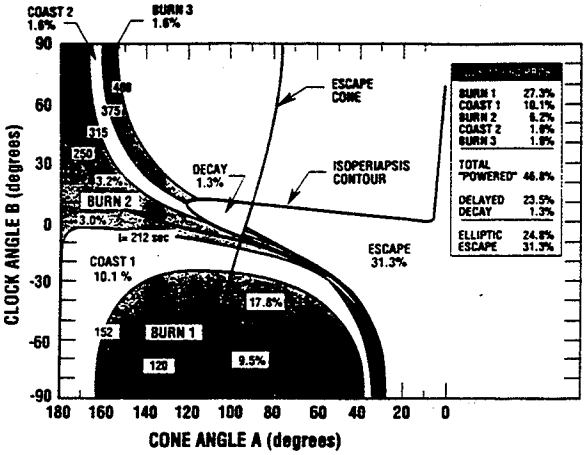

Fig. 7 Fixed misdirected burn map for Ulysses (analytic solution) for 110 n.mi. orbit.

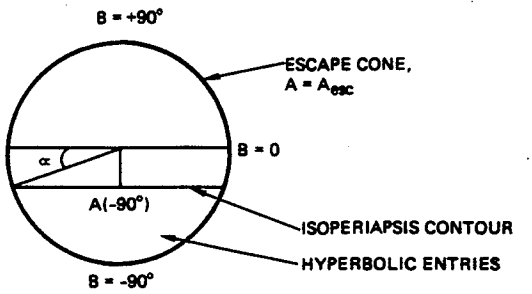

Fig. 8 Approximation for escape trajectories.

where

$$f = \tfrac{1}{2} + (\alpha + \sin\alpha \cos\alpha)/\pi$$

$$\alpha = \sin^{-1}\left[A(-90 \text{ deg})/A_{esc}\right]$$

and where $A(-90 \text{ deg})$ is defined by Eq. (17). (See Fig. 8.)

Spherical triangles[3,4] are used to approximate the area of orbit decay, since for low Earth orbits, the isoperiapsis contour can be approximated by great circles.

The area for the delayed entries is approximated by $(1-H-D)/2$ where H is the area of the escape cone and D is the area of the delay. No value is obtained for the prompt trajectories. Because of the slightly overestimated area for the total powered entries, the total of powered, elliptic, and escape is slightly greater than 100% for the analytic solutions.

Rotation of the impulsive burn contours (escape cone and periapsis contour) in the burn map of Fig. 7 is approximated by assuming a rotation angle of $\frac{1}{2}nt$, where the time t is now interpreted to be the total time from first ignition to final burnout, including coast times in between.

In comparing Figs. 6 and 7, we see that the analytic models capture the essential behavior of the burn plane. The average discrepancy between the numerical and analytic approaches is a few percent, with the greatest differences occurring for the minimum time for powered entries. (Of course, this is where we expect the greatest differences to show because there must be some cases where the analytic solution would just barely predict re-entry, while the numerical case would not.) In general the analytic solution tends to overestimate the powered entries.

Conclusions

An analytic model has been developed for the multistage injection problem. It shows good agreement with numerically generated plots and simplifies the analysis considerably. Both methods have their disadvantages and sources of error. The analytic method is limited by the linearized equations and other simplifying assumptions necessary to make the problem tractable. In the numerical approach, the accuracy is limited by the number of points selected on the burn plane for simulation, which is limited by the time (and patience) of the analyst. Because of these considerations, it is highly likely that both techniques have errors of the order of a few percent.

Perhaps the most profitable use of time is to use both methods in conjunction. The analytic burn plane can be produced first and requires only a few minutes to compute and plot. The results can be used to guide the selection of burn plane points in the numerical solution. Since the isochrones and the escape cone are approximated by small circles, a few one-dimensional searches in the burn plane may suffice to identify their locations and size. A similar approach may be used for the isoperiapsis contour. For small circles, numerical integration of the area is unnecessary. The area is found by measuring the radius of the circle and applying a simple formula.

In conclusion, the labor involved in the two-dimensional search on the burn plane can be reduced considerably in the numerical approach by using the analytic and geometric models developed here.

Acknowledgments

The author extends a special thanks to Angus D. McRonald for providing Fig. 6. The author also thanks Jean-Paul Berthias, Roger Diehl, Peter Jaffe, and Robert Mitchell for their valuable support.

References

[1]McRonald, A. D., "Galileo RTG Reentry Breakup Analysis," Jet Propulsion Lab., Mission Design Section, JPL Doc. 1625-228, Pasadena, CA, Sept. 1984.

[2]Jaffe, P., Diner, A., McRonald, A., and Tenn, L., "Ulysses Breakup Analysis Final Report," Jet Propulsion Lab., Applied Technologies Section, JPL Doc. 1628-54, Pasadena, CA, Nov. 1984.

[3]Longuski, J. M., "An Analytic-Geometric Model of the Effect of Spherically Distributed Injection Errors for the Galileo and Ulysses Spacecraft," American Astronomical Society, AAS Paper 87-487, AAS/AIAA Astrodynamics Conference, Kalispell, MT, Aug. 10–13, 1987.

[4]Longuski, J. M., and McRonald, A. D., "An Analytic-Geometric Model of the Effect of Spherically Distributed Injection Errors for Galileo and Ulysses Spacecraft: The Multi-Stage Problem," AIAA Paper 88-4245, AIAA/AAS Astrodynamics Conference, Minneapolis, Minnesota, Aug. 15–17, 1988.

[5]Kaplan, M. H., *Modern Spacecraft Dynamics & Control,* Wiley, New York, 1976, pp. 108–115.

[6]Greenwood, D. T., *Principles of Dynamics,* Prentice-Hall, Englewood Cliffs, NJ, 1965, Chap. 4.

[7]Kaplan, W., *Operational Methods for Linear Systems,* Addison-Wesley, Reading, MA, 1962, Chap. 2.